Materiales de Construcción
Vol. 66, Issue 323, July–September 2016, e091
ISSN-L: 0465-2746
http://dx.doi.org/10.3989/mc.2016.02915

Formation and early hydration characteristics of $C_{2.75}B_{1.25}A_3\$$ in binary system of $C_{2.75}B_{1.25}A_3\$$-C_2S

Shoude Wang✉, Yongbo Huang, Chenchen Gong, Xinghua Fu, Lingchao Lu

Shandong Provincial Key Lab. of Preparation and Measurement of Building Materials, University of Jinan, (Jinan, China)
✉personand98@163.com

Received 8 April 2015
Accepted 13 January 2016
Available on line 23 August 2016

ABSTRACT: $C_{2.75}B_{1.25}A_3\$$ (2.75CaO•1.25BaO• $3Al_2O_3$• SO_3) is one of the important minerals and it govern-directly the early-strength of belite-barium calcium sulphoaluminate cement. In this paper a binary system $C_{2.75}B_{1.25}A_3\$$-C_2S is selected to investigate the formation of $C_{2.75}B_{1.25}A_3\$$. In the range of 1100 °C–1200 °C, the earlier formed C_2S hinders the formation of $C_{2.75}B_{1.25}A_3\$$. On the contrary, when the temperature is in the range of 1200 °C–1350 °C, the initially formed C_2S could provide a surface for the nucleation of $C_{2.75}B_{1.25}A_3\$$ and cut down the potential barrier (ΔG_{k^*}) for the heterogeneous nucleation of $C_{2.75}B_{1.25}A_3\$$, which contributes to its formation. Moreover, at 1350 °C, the large amount of previously formed C_2S benefits the extent of formation of $C_{2.75}B_{1.25}A_3\$$. The possible reason was that it could prevent sulfur evaporation. In early hydration age, AFm and AFt originating from $C_{2.75}B_{1.25}A_3\$$ hydration are found within 2 h and 12 h under 95% RH at 1 °C, respectively, whereas C_2S is unhydrated at this moment.

KEYWORDS: Belite; Barium calcium suphoaluminate; Formation; Hydration; Early mechanical strength

Citation/Citar como: Shoude Wang; Yongbo Huang; Chenchen Gong; Xinghua Fu; Lingchao Lu. (2016) Formation and early hydration characteristics of $C_{2.75}B_{1.25}A_3\$$ in binary system of $C_{2.75}B_{1.25}A_3\$$-C_2S. *Mater. Construcc.* 66 [323], e091. http://dx.doi.org/10.3989/mc.2016.02915.

RESUMEN: *Formación y características de hidratación temprana del $C_{2.75}B_{1.25}A_3\$$ en el sistema binario de $C_{2.75}B_{1.25}A_3\$$-C_2S.* En el cemento de sulfoaluminato de calcio y bario, el $C_{2.75}B_{1.25}A_3\$$ (2.75CaO•1.25BaO• $3Al_2O_3$• SO_3) es una de las principales fases, y regula directamente la resistencia inicial del cemento. En este trabajo, se ha seleccionado el sistema binario $C_{2.75}B_{1.25}A_3\$$-C_2S para investigar la formación de $C_{2.75}B_{1.25}A_3\$$. En el rango de 1100 °C-1200 °C, el C_2S formado anteriormente impide la formación de $C_{2.75}B_{1.25}A_3\$$, mientras que cuando la temperatura está entre 1200 °C-1350 °C, el C_2S proporcionaría una superficie de nucleación de $C_{2.75}B_{1.25}A_3\$$ reduciendo la barrera de potencial (ΔG_{k^*}) para la nucleación heterogénea de $C_{2.75}B_{1.25}A_3\$$, lo que contribuye a su formación. Además, a 1350 °C, la gran cantidad de C_2S formado beneficia la formación de $C_{2.75}B_{1.25}A_3\$$, ya que podía prevenir la evaporación del azufre. En las primeras etapas de la hidratación (entre 2 y 12h y 95% HR a 1 ºC) se pueden encontrar AFM y AFt procedentes de la hidratación de $C_{2.75}B_{1.25}A_3\$$, mientras que el C_2S permanece sin hidratar.

PALABRAS CLAVE: Belita; sulfoaluminato de calcio y bario; Formación; Hidratación; Resistencias mecánicas tempranas

1. INTRODUCTION

The Portland cement (PC) clinker manufacture consumes about 2900 to 3300 MJ per ton of clinker (1), which is considered to heat the raw meal to a temperature exceeding 1450 °C that allows alite phase to form (2). Moreover, around 830–970 kg CO_2 per ton (3, 4) are emitted of clinker in direct (5–7) and indirect ways (8, 9), which brings about enormous environmental footprint (6). In short, the cement industry is responsible for 5–7% of all anthropogenic emissions (10, 11) world wide. In order to attain sustainable development for manufacture of PC, there has been a revival of intensive interests in exploring high belite cement with low lime saturation factor (LSF), which leads to an increase in belite amount and a decrease in alite phase content in the clinker (12–16).

However, C_2S, even with high activity form (17, 18), is less active than C_3S, which has become the most significant limitation for the extensive application of belite cement (17, 19). Thus, many investigations were performed in an attempt to introduce another high early-strength mineral with low CaO such as $C_4A_3\$$ (20–23) or $C_{2.75}B_{1.25}A_3\$$ ($2.75CaO•1.25BaO•3Al_2O_3•SO_3$) (24, 25) into belite cement clinker system. Compared with $C_4A_3\$$, $C_{2.75}B_{1.25}A_3\$$, it possesses much higher early-strength (26, 27). Consequently, belite-$C_{2.75}B_{1.25}A_3\$$ system, with the designed composition of 9.0% $C_{2.75}B_{1.25}A_3\$$, 75% silicate mineral and 16% intermediate phase (by weight, as following) (28, 29), has the potential to receive attention nowadays.

In belite-$C_{2.75}B_{1.25}A_3\$$ system, the formation of $C_{2.75}B_{1.25}A_3\$$ governed directly the early-strength of cement clinker. Consequently, it is necessary to reveal the influence of silicates and intermediate phases on the formation of $C_{2.75}B_{1.25}A_3\$$, which is not explored in previous work. On account of the belite as one of the main phases and the complication of phase composition for this new type of cement clinker system, the binary system of C_2S-$C_{2.75}B_{1.25}A_3\$$ was designed to gain a deep insight into the effect of the high content of C_2S on the formation of $C_{2.75}B_{1.25}A_3\$$. Furthermore, for that the early mechanical property of belite cement is connected with its early hydration characteristics, the hydration and evolution process of this binary system is monitored by ESEM at early stage. Moreover, this research also lays foundation for the basic study of sulphoaluminate mineral modified silicate cement.

2. EXPERIMENTAL

2.1. Specimens Preparation

The used chemicals $CaCO_3$, Al_2O_3, SiO_2, $BaCO_3$ and $BaSO_4$ were reagent grade, which come from Sinopharm Chemical Reagent Co., Ltd, China. All regents were weighted accurately according to the anticipated proportion (Table 1) to obtain the mixtures. The mixtures were blended uniformly with water by planetary ball mill and placed in the drying oven at 105 °C for 4 h. After that, they were pressed into discs with the size of 40 mm×40 mm×3 mm at 10MPa. Then the discs were heated to different high temperatures (1000 °C, 1100 °C, 1150 °C, 1200 °C, 1250 °C, 1300 °C and 1350 °C) for 2 hours with the rise speed of 5 °C per minute in high temperature furnace and cooled with forced air rapidly. Finally, the specimens were ground to pass 200 mesh sieve for the next analysis.

Three kinds of specimens were prepared in this experiment. The binary system clinker of C_2S-$C_{2.75}B_{1.25}A_3\$$ (37.5:9.0 in weight) was synthesized and named as specimen No.1. Moreover, the pure minerals of $C_{2.75}B_{1.25}A_3\$$ and C_2S were also fabricated and named as the reference specimen No.2 and No.3 respectively. Due to the solid solution of BaO and SO_3 (30), excessive 6.44wt% (as carbonate) $BaCO_3$ and 4.41wt% (as sulfate) $CaSO_4$ (taking the extra calcium into consideration) were added into the raw material of specimen No.1. Table 1 displays the proportioning of the specimens.

2.2. Specimen testing

Free lime displays the burnability of the specimen. F-CaO content of the specimens was determined by ethanol-glycerin method. X-ray diffraction analysis was performed by X-ray diffraction (D8 Advance, Germany) using Cu Kα radiation with an increment of 0.01° and maintaining time of 0.5s at a voltage of 40 kv and current of 40mA in 5-60 2θ range. The DSC-TGA analysis was carried out by a simultaneous thermal analyzer (TGA/DSC1/1600HT, Germany) with heating rate of 10 °C·min^{-1} in flowing Ar at rate of 50 ml·min^{-1}. FT-IR spectroscopy analysis was conducted by infrared spectrometer (Nicolet 380, America) with a detector DGTS CsI and 32 scans were recorded to register each specimen. The scans were taken in the mid-infrared region at frequencies of 4000 cm^{-1} to 400 cm^{-1}, with a spectral resolution of 4 cm^{-1}. Specimens for SEM-EDS analysis were prepared by cutting with a diamond saw and polishing with silicon carbide discs. The prepared samples were coated with 12 nm thick gold and examined by field emission scanning electron microscopy (SEM: QUANTAFEG, America;

Table 1. Proportioning of the specimens (g/100g specimen)

Specimens	$CaCO_3$	SiO_2	Al_2O_3	$BaSO_4$	$BaCO_3$
No.1	97.77	24.13	8.09	6.17	1.30
No.2	37.61	—	41.80	31.89	6.74
No.3	116.22	34.88	—	—	—

EDS: INCA, England) at a voltage of 20 kv and current of 20 mA. Specimen for ESEM analysis did not require special treatment. Early stage hydration characteristics of specimen No.1 prepared at 1350 °C were monitored by ESEM with Carl Zeiss EVO 15. The morphology of water drops and the ternary phase diagram of H_2O were shown in Figure 1. When the work condition of ESEM was controlled at the center of the shuriken in the phase diagram, specimen in the chamber was subjected to a relative humidity (RH) of 95% and 1 °C. Moreover, six specimens were used for the determination of the measure data.

2.3. Quantitative analysis

Due to the fact that so far we do not have the crystal structure parameter of $C_{2.75}B_{1.25}A_3$\$, reference intensity ratio (RIR) method is chosen to quantify the mineralogical data. This is one of the most simple and quickest ways to quantify X-ray diffraction data (31) and it has been proven effective in the quantification of mineralogical data (32). To confirm the weight fraction of $C_{2.75}B_{1.25}A_3$\$ mineral in specimen No.1 and No.2, RIR method was conducted. Mixtures were prepared by mixing specimen No.1 and No.2 with CaF_2 in the weight ratio of 10:1. This mixture was dispersed in a 0.5% (w/v) aqueous solution of polyvinyl alcohol to form a suspension in which the solid-to-liquid ratio was 1:2. The suspension was spray dried at 105 °C and the collected particles were used for the quantitative analysis using the RIR method. The pure $C_{2.75}B_{1.25}A_3$\$ mineral used in the quantitative analysis was fabricated by sintering the discs at 1350 °C for 4 h (33).

Figure 2 shows the XRD pattern of specimen No.1 and No.2 sintered at 1000 °C. From Figure 2, it is noticed that a certain amount of aluminate mineral (CA and $C_{12}A_7$) forms in specimen No.1 and No.2 at 1000 °C. Meanwhile, not any obvious f-CaO characteristic peaks are detected in specimen No.2, while three obvious f-CaO characteristic peaks appear in specimen No.1. So the majority of f-CaO used to form $C_{2.75}B_{1.25}A_3$\$ was consumed at 1000 °C. In addition, the f-CaO content considered to form $C_{2.75}B_{1.25}A_3$\$ is no more than 4.0% in specimen No.1 by weight. Therefore, it is reasonable to regard the f-CaO in specimen No.1 as the part which is applied to form C_2S. Therefore, it is reasonable to calculate the extent of formation of C_2S in specimen No.1 and No.3 by indirectly or directly using the following equation Eq.[1]:

$$\alpha = 1 - \frac{\text{f-CaO}}{\text{f-CaO}_{C2S}} \qquad [1]$$

Where α is the extent of formation of C_2S and f-CaO_{C2S} is the CaO content in $2CaO{\bullet}SiO_2$. For specimen No.3, f-CaO is the lime content of the specimen at any temperature. For specimen No.1, f-CaO is 5.17 times the lime content of specimen No. 2 at any temperature.

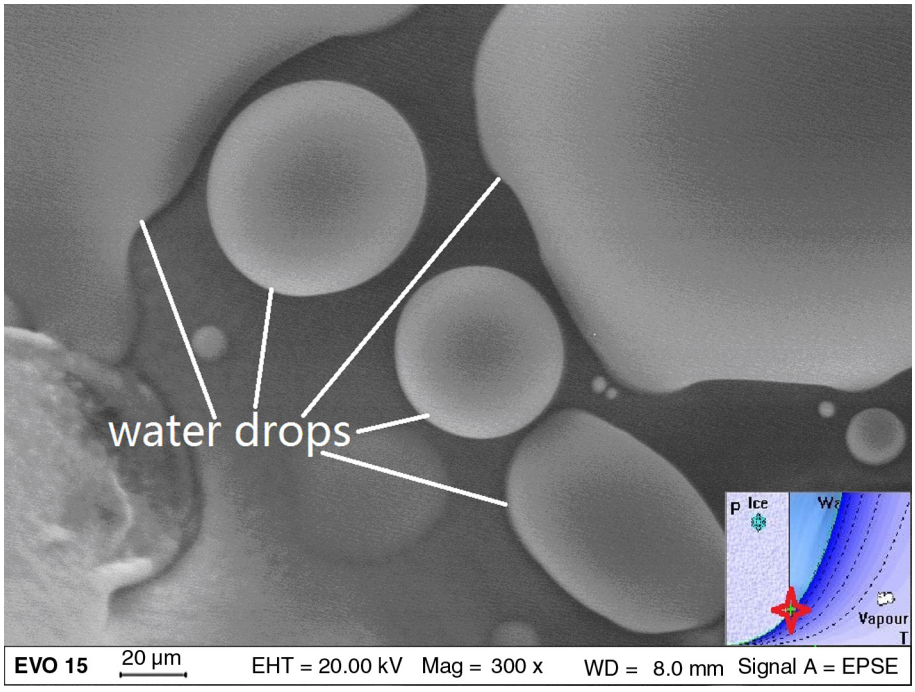

FIGURE 1. Morphology of water drops and the ternary phase diagram of H_2O.

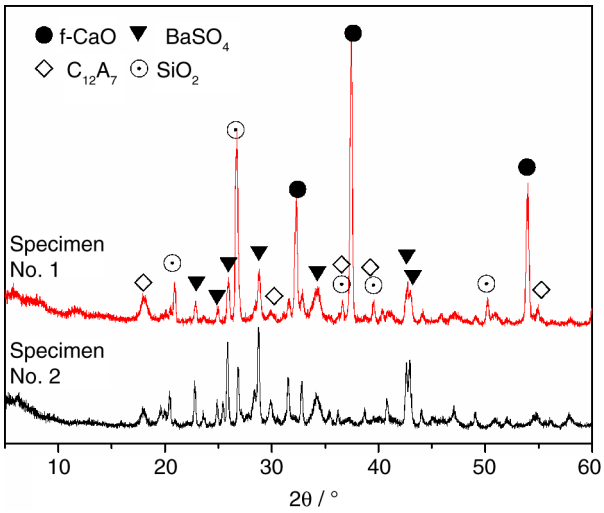

FIGURE 2. XRD patterns of specimens No.1 and No.2 sintered at 1000 °C.

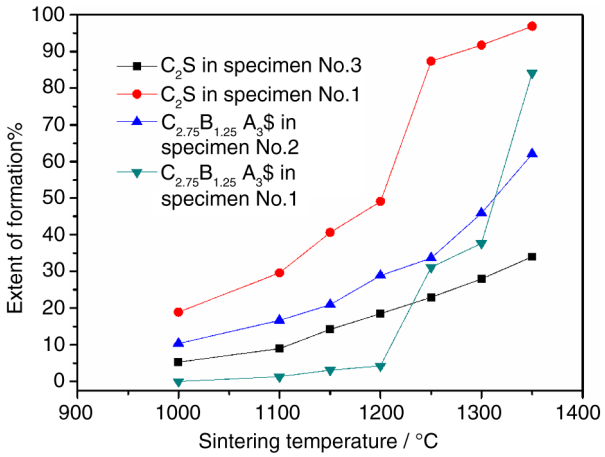

FIGURE 3 Extent of formation of $C_{2.75}B_{1.25}A_3\$$ and C_2S in the specimens.

3. RESULTS AND DISCUSSION

3.1. Variation of phase composition

3.1.1. Extent of formation

To inspect the effect of C_2S on the formation mechanism of $C_{2.75}B_{1.25}A_3\$$ mineral, the extent of formation of $C_{2.75}B_{1.25}A_3\$$ in the specimen No.1 and No.2 were measured by the RIR method. The methodology used to calculate the extent of formation of C_2S is based on the assumption that the free CaO in specimen No.1 belonged to the part applied to form C_2S. This methodology has been proven in the experimental part. It is highlighted that free CaO content is a key factor for the quantitative analysis of C_2S. Due to its easy hydration, it is mandatory to perform the free CaO content test immediately after the sintering of the specimens.

A comparison of the extent of formation of $C_{2.75}B_{1.25}A_3\$$ and C_2S in specimen No.1, No.2 and No.3 is shown in Figure 3. It is observed that in the range of 1000 °C to 1200 °C, the extent of formation of C_2S in specimen No.1 is relatively higher than that in specimen No.3. In particular, when sintering temperature proceeds in the range of 1200 °C to 1350 °C, C_2S can form in a much faster rate in specimen No.1 than in specimen No.3. As for $C_{2.75}B_{1.25}A_3\$$ mineral, in the range of 1000 °C to 1200 °C, its rate of formation in specimen No.1 is much slower than in specimen No.2. When the temperature changes into the range of 1200 °C to 1350 °C, the extent of formation of $C_{2.75}B_{1.25}A_3\$$ in specimen No.1 increases much faster than in specimen No.2. Eventually, the extent of formation of $C_{2.75}B_{1.25}A_3\$$ in specimen No.1 exceeds that of specimen No.2 at 1350 °C.

3.1.2. X ray diffraction analysis

Figure 4 illustrated the XRD patterns of specimen No.1 sintered at different temperatures. As shown in Figure 4 (a), in the range of 1100–1200 °C, the main phases are $BaSO_4$ and free CaO. Also, slight amounts of intermediate phases, such as BA, CA and $C_{12}A_7$, are found. The characteristic peaks of $C_{2.75}B_{1.25}A_3\$$ and C_2S are detectable but weak at 1200 °C. As seen from Figure 3 (a) and (b), in the range of 1250–1350 °C, the diminution of diffraction peaks of free CaO and the appearance of characteristic peaks of β-C_2S and γ-C_2S can be observed, proving that a large amount of C_2S is formed. From Figure 4 (b) and (c), it is seen that with the rise of sintering temperature, the intensity of characteristic peaks of β-C_2S increases, while the intensity of characteristic peaks of γ-C_2S displays a contrary tendency. Ultimately, the characteristic peaks of γ-C_2S are not detectable in specimen No.1 sintered at 1350 °C, due to its absence or small content. In specimen No.3, γ-C_2S is the main polymorph. This is different from that in specimen No.1, whose main polymorph is β-C_2S. The reason is the partial substitution of Ba^{2+} and $[SO_4]^{4-}$ for Ca^{2+} and $[SiO_4]^{4-}$ in C_2S, which results in a rise in both disorder state of lattice and entropy of the system (19) and supports the maintenance of high temperature form of β-C_2S at ambient temperature (3, 7, 34). As shown from Figure 4 (a) and (c), it is observed that the intensity of the characteristic peak for $C_{2.75}B_{1.25}A_3\$$ (3.7888 Å, 2.2010 Å, 1.9494 Å) increases rapidly at 1350 °C. Meanwhile, the characteristic peaks of BA, CA and $C_{12}A_7$ disappear simultaneously. Combination with the discussion of previous works (35), this indicated that the formation of $C_{2.75}B_{1.25}A_3\$$ mineral is sufficient.

a. 5°-60° range
b. 22°-24° range and 29°-40° range
c. 40°-50° range

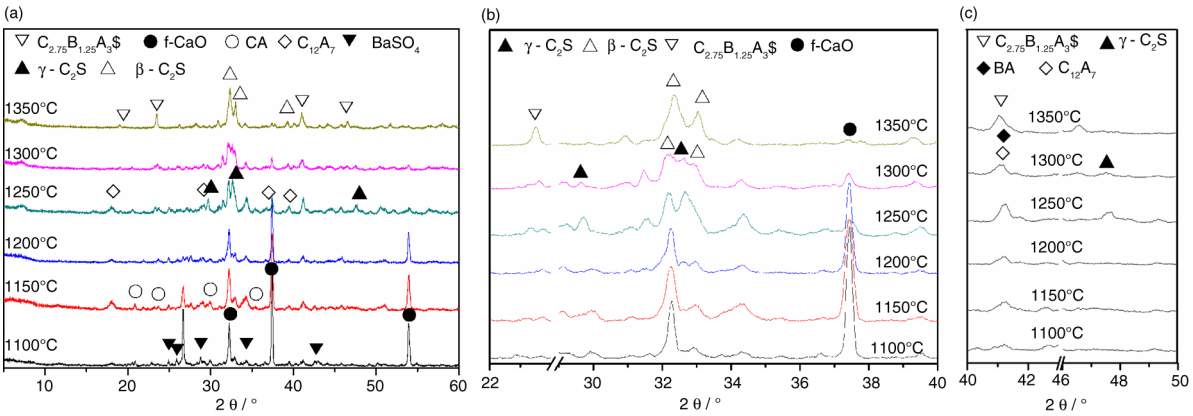

FIGURE 4. XRD patterns of specimen No.1 sintered at different temperature.

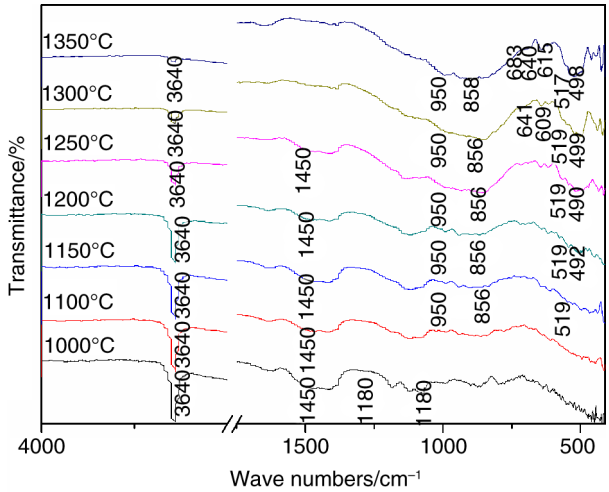

FIGURE 5. FT-IR spectrum of specimen No.1.

3.1.3. *FT-IR spectrum analysis*

The FT-IR spectrum shows the main absorption band and identification group of the functional group. The FT-IR results for specimens sintered at different temperatures is illustrated in Figure 5. As shown in Figure 5, at high wave-number stage the major absorption peaks concentrate at 3640 cm^{-1}, which is assigned to the vibration of [OH]. The reason is that partial f-CaO reacts with H_2O and generates $Ca(OH)_2$ during the time of the preservation of the specimens. The above mentioned absorption peak intensity presents a decreasing trend with the rise of temperature, indicating the reduction of CaO content in the specimen. The result is in accordance with the X-ray diffraction analysis. At 1000 °C, $BaCO_3$ decomposes thoroughly (35). Therefore, the vibration band at 1450 cm^{-1} is mainly attributed to the portlandite carbonation. The vibration band at 1180 cm^{-1} and 1080 cm^{-1} is mainly due to the asymmetric stretching vibration of [SO_4].

As shown in Figure 5, the asymmetric stretching vibration of [SiO_4] tetrahedron of C_2S is displayed at 856 cm^{-1}–950 cm^{-1}. When the sintering temperature exceeds 1350 °C, the peak becomes more and more obvious, which indicates that a large amount of C_2S is formed. The bending vibration of [SO_4] tetrahedron sites at 600 cm^{-1}–700 cm^{-1}. Owing to the bending coupling vibration of [SO_4] tetrahedron and [AlO_4] tetrahedron, obvious peaks emerge at 683 cm^{-1}, 640 cm^{-1} and 615 cm^{-1} (36) when the sintering temperature is 1350 °C, indicating that $C_{2.75}B_{1.25}A_3\$$ can form perfectly at this temperature. All of the above stated results are identical with those acquired from the XRD analysis.

3.1.4. *Differential scanning calorimetric analysis*

Differential scanning calorimetric analysis is applied to monitor the evolution of solid phase reaction during the processing of the raw meals being sintered. The heat evolution during the process of sintering the specimen is illustrated in Figure 6. Decomposition of $CaCO_3$ is characterized by evident endothermic peak at 600–850 °C. The beginning temperature for the decomposition of $CaCO_3$ in specimen No.1 is almost identical with that of specimen No.3, but the terminated temperature lowers down sharply from 865 °C to 835 °C, proving that $CaCO_3$ decomposition rate is promoted in specimen No.1. As seen from Figure 6, an obvious exothermal peak attributed to the formation of β-C_2S shows at around 1360 °C in the curve of specimen No.3. Due to no mineralizer, its formation temperature is relatively higher than that in cement clinker. By contrast, the dispersed exothermal peak corresponding to the formation of β-C_2S in the curve of specimen No.1 shows at around 1270 °C, which is prior to the formation of β-C_2S in specimen No.3.

This is due to the existence of Ba and S element, which tends to lower down the eutectic point of the system. A strong and sharp endothermal peak

due to the decomposition of $C_{2.75}B_{1.25}A_3\$$ mineral is displayed at around 1370 °C in the curve of specimen No.2. While at the same temperature, no such peak is observed in the curve of specimen No.1. Consequently, we come to a conclusion that the decomposition of $C_{2.75}B_{1.25}A_3\$$ in specimen No.1 is postponed or inhibited.

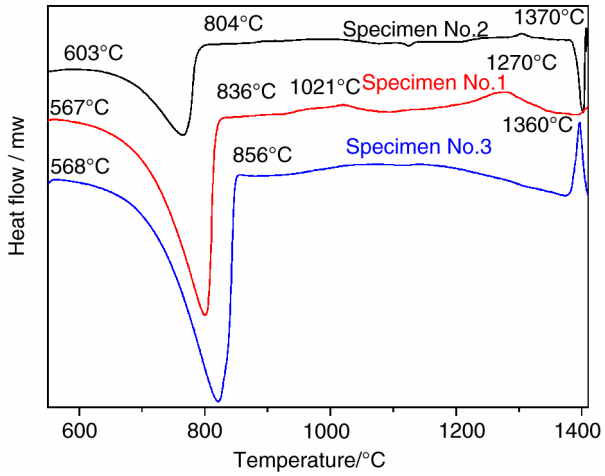

FIGURE 6. DSC curve of the specimens.

3.2. Phases growth and distribution in the binary system

Textual relationships, mineral grain morphology and elemental distribution were studied by SEM images and EDS spectra. Figure 7 shows two representative SEM images and four EDS spectra of specimen No.1 obtained at 1350 °C. The EDS result proves that the mass at point '1'position presenting red blood cell shape with a hole in the middle is $C_{2.75}B_{1.25}A_3\$$ and the mass at point '2'position is belite solid solution (partial substitution of Ba and S for Ca and Si in C_2S). Therefore, it is concluded that C_2S and $C_{2.75}B_{1.25}A_3\$$ can coexist in the binary system.

3.3. Formation mechanism discussions

In the range of 1100 °C–1200 °C, the primarily formed C_2S is not conductive to the combination of calcium, barium, aluminum and sulfur from hindering the formation of $C_{2.75}B_{1.25}A_3\$$. It explains the reason why the extent of formation of $C_{2.75}B_{1.25}A_3\$$ in specimen No.1 is relatively lower in the temperature range of 1100 °C-1200 °C. As is known to all, crystal formation undergoes the following two steps of nucleation and crystal embryos

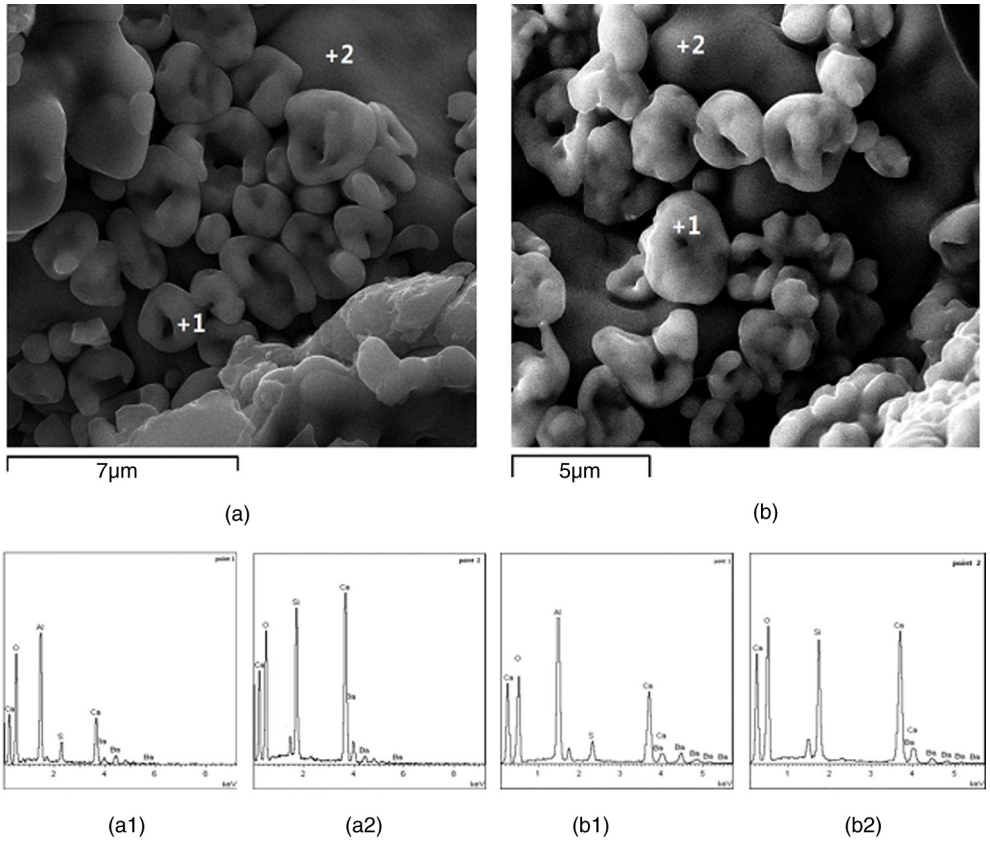

FIGURE 7. SEM and EDS analysis of specimen 1 sintered at 1350 °C.

growth (37). Nucleation normally can be classified to two categories of heterogeneous nucleation and homogeneous nucleation. Heterogeneous nucleation tends to nucleate on the surface, interface and wall of container, which contributes to cutting down the potential barrier (ΔG_k^*) of the heterogeneous nucleation. X ray diffraction analysis and FT-IR spectrum analysis indicate that the large amount formation temperature of C_2S and $C_{2.75}B_{1.25}A_3\$$ are 1250 °C and 1350 °C respectively. Therefore, in the range of 1200 °C-1350 °C, primarily formed C_2S can provide surface for the nucleation of $C_{2.75}B_{1.25}A_3\$$, which cuts down the ΔG_k^* for the heterogeneous nucleation of $C_{2.75}B_{1.25}A_3\$$. Besides, the condition of high temperature can boost the frequency of collisions between elements of calcium, barium, aluminum and sulfur which are considered to form $C_{2.75}B_{1.25}A_3\$$. The above stated interprets the growth

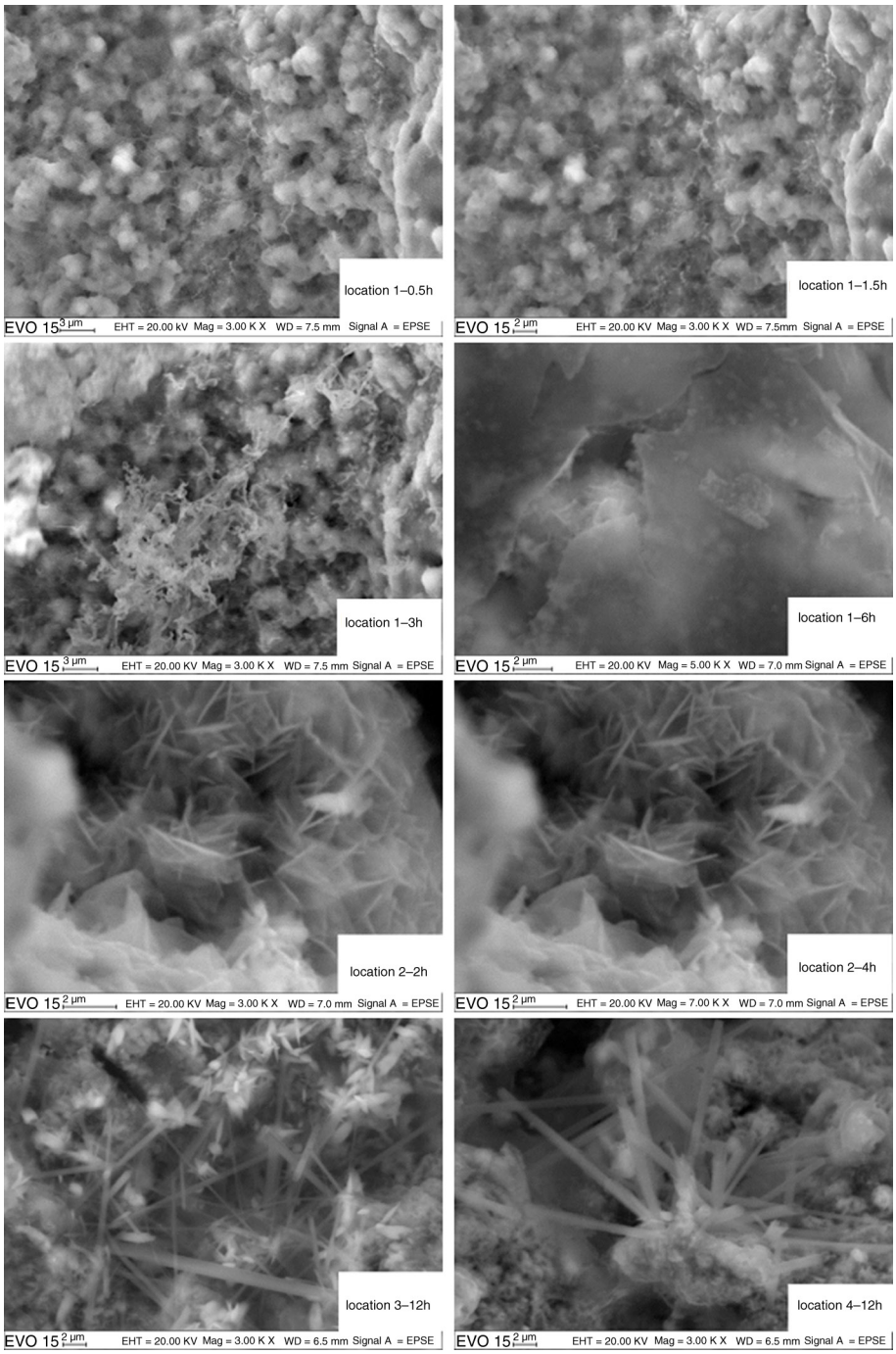

FIGURE 8. ESEM micrographs of specimen No.1 sintered at 1350 °C.

rhythm of $C_{2.75}B_{1.25}A_3\$$ and the reason why the rate of extent of formation of $C_{2.75}B_{1.25}A_3\$$ in specimen No.1 is relatively higher in the temperature range of 1200 °C-1350 °C. At 1350 °C, the extent of formation of $C_{2.75}B_{1.25}A_3\$$ in specimen No.1 exceeds that in specimen No.2. It may attribute to that the large amount of previously formed C_2S prevent sulfur element from evaporation, which is benefit to the formation of $C_{2.75}B_{1.25}A_3\$$ (38).

3.4. Characteristics of early hydration

Figure 8 displays the hydration process of specimen No.1 without $CaSO_4·2H_2O$ monitored by ESEM under the condition of 95% RH and 1 °C. As shown from Figure 8, four locations of specimen are analyzed. From the micrographs of random location 1 at 0.5 h, 1.5 h, 3 h, it is easy to notice the interlocking of the hydration products, which is always dominating the setting of cement (21). At 6 h, it is observed that a continuous hydration film is formed on the surface of specimen, which are consist of hydrated calcium sulphoaluminate and alumina gel. From the micrographs of location 2 at which much $C_{2.75}B_{1.25}A_3\$$ mineral exists, flake monosulfate (AFm, $3CaO·Al_2O_3·CaSO_4·12H_2O$) is observed after 2 h. With the prolonging of curing time, no ore AFm forms is observed at 4 h, proving that AFm mainly forms within 2 h. With hydration time prolonging, the amount of AFm does not increase significantly. This means that AFm could form sufficiently. However, from the micrographs of typical location 3 and 4, minor AFt with needle shape is observed after 12 h. Previous investigation also found that the main hydrate of $C_{2.75}B_{1.25}A_3\$$ in belite-barium calcium sulphoaluminate cement with 8% $CaSO_4·2H_2O$ is ettringite (AFt, $3CaO·Al_2O_3·3CaSO_4·32H_2O$) (26). Therefore, it is reasonable to speculate that the solid solution of sulphur for belite in the binary system lowers down, which inevitably leads to an excessive amount of sulphur in the specimen No.1 and promotes the formation of AFt. At hydration age of 12 h, no plate $Ca(OH)_2$ is found in Figure 8. This indicates that C_2S mineral is unhydrated at this stage.

4. CONCLUSIONS

In the range of 1100 °C-1200 °C, the primarily formed C_2S is not conductive to the element combination of calcium, barium, aluminum and sulfur, hindering the formation of $C_{2.75}B_{1.25}A_3\$$. It explains the reason why the extent of formation of $C_{2.75}B_{1.25}A_3\$$ in the binary system is low in this temperature range. On the contrary, when the temperature is in the range of 1200 °C-1350 °C, the primarily formed C_2S contributed to the formation of $C_{2.75}B_{1.25}A_3\$$, which could provide surface for the nucleation of $C_{2.75}B_{1.25}A_3\$$ and cut down the potential barrier (ΔG_k^*) for the heterogeneous nucleation of $C_{2.75}B_{1.25}A_3\$$. Besides, the condition of high temperature can boost the collision frequency of the elements of calcium, barium, aluminum and sulfur. The above stated phenomenon facilitates the formation of $C_{2.75}B_{1.25}A_3\$$. At 1350 °C, the extent of formation of $C_{2.75}B_{1.25}A_3\$$ in specimen No.1 exceeds that in specimen No.2. This may attribute to the fact that the large amount of previously formed C_2S prevent sulfur element from evaporation, which is a benefit to improve the extent of formation for $C_{2.75}B_{1.25}A_3\$$. In early hydration age, AFm and AFt originating from $C_{2.75}B_{1.25}A_3\$$ hydration are found within 2 h and 12 h under 95% RH at 1 °C, respectively, whereas C_2S is unhydrated at this moment.

ACKNOWLEDGEMENTS

This work is supported by Natural Science Foundations of China (Grant 51272091) and Shandong Province Bold Talent program (ZR2015EM002). Meanwhile, this work was supported by Program for Scientific Research Innovation Team in Colleges and Universities of Shandong Province.

REFERENCES

1. Schneider M.; Romer M.; Tschudin M.; Bolio H. (2011) Sustainable cement production-present and future. *Cem. Concr. Res.* 41 [7], 642-650. http://dx.doi.org/10.1016/j.cemconres.2011.03.019.
2. Kacimi L.; Simon M. A. ; Ghomaric A.; Derrichea Z. (2006) Reduction of clinkerization temperature by using phosphogypsum. *J. Hazard. Mater.* 137 [1], 129–137. http://dx.doi.org/10.1016/j.jhazmat.2005.12.053.
3. Worrell E.; Price L.; Martin N.; Hendriks C.; Meida L.O. (2001) Carbon dioxide emissions from the global cement industry. *Annu. Rev. Energy Env.* 26, 303-329. http://dx.doi.org/10.1146/annurev.energy.26.1.303.
4. Benhelal E.; Zahedi G.; Shamsaei E.; Bahadori A. (2013) Global strategies and potentials to curb CO_2 emissions in cement industry. *J. Clean. Prod.* 51 [15], 142-161. http://dx.doi.org/10.1016/j.jclepro.2012.10.049.
5. Morsli K.; De la Torre A.G.; Zahir M.; Aranda M.A. (2007) Mineralogical phase analysis of alkali and sulfate bearing belite rich laboratory clinkers. *Cem. Concr. Res.* 37 [5], 639-646. http://dx.doi.org/10.1016/j.cemconres.2007.01.012.
6. García-Díaz I.; Palomo J.G.; Puertas F. (2011) Belite cements obtained from ceramic wastes and the mineral pair $CaF_2/CaSO_4$. *Cem. Concr. Compos.* 33 [10], 1063-1070. http://dx.doi.org/10.1016/j.cemconcomp.2011.06.003.
7. Y.T. Zhao; L.C. Lu; S.D. Wang; C.C. Gong; Y.B. Huang. (2013) Modification of dicalcium silicates phase composition by BaO, SO_3 and MgO, J. Inorg. Organomet. Polym. Mater. 23 [4], 930-936. http://dx.doi.org/10.1007/s10904-013-9873-2.
8. Yang L.; Yan Y.; Hu Z.H.; Xie X.L. (2013) Utilization of phosphate fertilizer industry waste for belite-ferroaluminate cement production. *Constr. Build. Mater.* 38, 8-13. http://dx.doi.org/10.1016/j.conbuildmat.2012.08.049.
9. Chen Y.L. ; Lin C.J. ; Ko M.S. ; Lai Y.C. ; Chang J.E. (2011) Characterization of mortars from belite-rich clinkers produced from inorganic wastes. *Cem. Concr. Compos.* 33 [2], 261-266. http://dx.doi.org/10.1016/j.cemconcomp.2010.10.012.

10. Ali M.B.; Saidur R.; Hossain M.S. (2011) A review on emission analysis in cement industries. Renew. Sust. Energ. Rev. 15, 2252-261. http://dx.doi.org/10.1016/j.rser.2011.02.014.
11. IEA(International Energy Agency), WBCSD(World Business Council for Sustainable Development).Cement technology roadmap 2009: carbon emissions reductions up to 2050. (2009) http://www.iea.org/papers/2009/Cement_Roadmap.pdf.
12. Chen Y.L.; Shih P.H.; Chiang L.C.; Chang Y.K.; Lu H.C.; Chang J.E. (2009) The influence of heavy metals on the polymorphs of dicalcium silicate in the belite-rich clinkers produced from electroplating sludge. *J. Hazard. Mater.* 170 [1], 443-448. http://dx.doi.org/10.1016/j.jhazmat.2009.04.076.
13. Chen I.A.; Juenger M.C.G. (2011) Synthesis and hydration of calcium sulphoaluminate-belite cements with varied phase compositions. *J. Mater. Sci.* 46 [8], 2568-2577. http://dx.doi.org/10.1007/s10853-010-5109-9.
14. Lu L.C.; Zhao P.Q.; Wang S.D.; Chen Y.M. (2011) Effect of Calcium carbide residue and high silicon limestone on the synthesis of belite-barium calcium sulphoaluminate cement. *J. Inorg. Organomet. Polym.* 21 [4], 900-905. http://dx.doi.org/10.1007/s10904-011-9560-0.
15. Lacobescu R.I. ; Koumpouri D. ; Pontikes Y. ; Saban R. ; Angelopoulos G.N. (2011) Valorisation of electric arc furnace steel slag as raw material for low energy belite cements. *J. Hazard. Mater.* 196 [30], 287-294. http://dx.doi.org/10.1016/j.jhazmat.2011.09.024.
16. Pimraksa K.; Hanjitsuwan S.; Chindaprasirt P. (2009) Synthesis of belite cement from lignite fly ash. *Ceram. Int.* 35 [6], 2415-2425. http://dx.doi.org/10.1016/j.ceramint.2009.02.006.
17. Kacimi L.; Cyr M.; Clastres P. (2010) Synthesis of α'-C_2S cement from fly-ash using the hydrothermal method at low temperature and atmospheric pressure. *J. Hazard. Mater.* 181 [1-3], 593-601. http://dx.doi.org/10.1016/j.jhazmat.2010.05.054.
18. Sharp J.H.; Lawrence C.D.; Yang R. (1999) Calcium sulphoaluminate cements-low energy cements, special cements or what? *Adv. Cem. Res.* 11 [1], 3-13. http://dx.doi.org/10.1680/adcr.1999.11.1.3.
19. Kacimi L.; Simon M.A.; Salem S.; Ghomari A.; Derriche Z. (2009) Synthesis of belite cement clinker of high hydraulic reactivity. *Cem. Concr. Res.* 39 [7], 559-565. http://dx.doi.org/10.1016/j.cemconres.2009.02.004.
20. Stephane B.; Celine C.D.C.; Patrick L.B.; Damidot D. (2011) Influence of a thermal cycle at early age on the hydration of calcium sulphoaluminate cements with variable gypsum contents. *Cem. Concr. Res.* 41 [2], 149-160. http://dx.doi.org/10.1016/j.cemconres.2010.10.001.
21. Pelletier C.L.; Winnefeld F.; Lothenbach B.; Saout G. L.; Jörg Müller C.; Famy C. (2011) Influence of the calcium sulphate source on the hydration mechanism of Portland cement-calcium sulphoaluminate clinker–calcium sulphate binders. *Cem. Concr. Compos.* 33 [5], 551-561. http://dx.doi.org/10.1016/j.cemconcomp.2011.03.005.
22. Liu X.C.; Li Y.J.; Zhang N. (2002) Influence of MgO on the formation of Ca_3SiO_5 and $3CaO{\cdot}3Al_2O_3{\cdot}CaSO_4$ minerals in alite-sulphoaluminate cement. *Cem. Concr. Res.* 32 [7], 1125-1129. http://dx.doi.org/10.1016/S0008-8846(02)00751-2.
23. Martin-Sedeno M.C.; Cuberos A.J.M.; De la Torre A.G. ; Álvarez-Pinazo G.; Ordónez L.M.; Gateshki M.; Aranda M.A.G. (2010) Aluminum-rich belite sulfoaluminate cements: Clinkering and early age hydration. *Cem. Concr. Res.* 40 [3], 359-369. http://dx.doi.org/10.1016/j.cemconres.2009.11.003.
24. Cheng X.; Chang J.; Lu L.C.; Liu F.T.; Teng B. (2000) Study of Ba-bearing calcium sulphoaluminate minerals and cement. *Cem. Concr. Res.* 30 [1], 77-81. http://dx.doi.org/10.1016/S0008-8846(99)00204-5.
25. Cheng X.; Chang J.; Lu L.C.; Liu F.T.; Teng B. (2004) Study on the hydration of Ba-bearing calcium sulphoaluminate in the presence of gypsum. *Cem. Concr. Res.* 34 [11], 2009-2013. http://dx.doi.org/10.1016/j.cemconres.2004.02.021.
26. Lu L.C.; Wang H.; Wang S.D.; Guo X.Y. (2010) Influence of MgO on sintering and property of belite-barium calcium sulphoaluminate cement. *J. Build. Mater.* 13 281-285. http://dx.doi.org/10.3969/j.issn.1007-9629.2010.03.002.
27. Lu L.C.; Zhang W.W.; Xuan H.Z.; Cheng X. (2008) Calcination condition of belite-calcium barium sulphoaluminate cement and its performance. *J. Chin. Ceram. Soc.* 36 165-169. http://dx.doi.org/10.14062/j.issn.0454-5648.2008.s1.038.
28. Zhang W.W.; Lu L.C.; Cui Y.J.; Chang J.; Cheng X. (2007) Microstructure and performances of belite-calcium barium sulphoaluminate cement. *J. Chin. Ceram. Soc.* 35 467-471. http://dx.doi.org/10.14062/j.issn.0454-5648.2007.04.015.
29. Zhao P.Q.; Lu L.C.; Wang S.D. (2011) Influence of high-silicon limestone on mineral structure and performance of belite-barium calcium sulphoaluminate clinker. *Adv. Mater. Res.* 168-170, 460-465. http://dx.doi.org/10.4028/www.scientific.net/AMR.168-170.460.
30. Wang Z.; Ba H.J.; Li J.H.; Zhang Y.Z. (2005) Effect of solid solubility of hetero-iron properties of high-belite cement, *J. Wuhan Univ. Tech.* 27, 33-35. http://dx.doi.org/10.1007/s11595-009-5834-6.
31. Johoson Q.; Zhou R.S. (1998) Checking and estimating RIR values, *International Centre for Diffraction Data 2000, Advances in X-ray Analysis*, 42, 233-239.
32. Ottner F.; Gier S.; Kuderna M.; Schwaighofer B. (2000) Results of an inter-laboratory comparison of methods for quantitative clay analysis, *Applied Clay Science,* 17 [5-6], 223-243. http://dx.doi.org/10.1016/S0169-1317(00)00015-6.
33. Huang Y.B.; Wang S.D.; Gong C.C.; Zhao Y.T.; Lu L.C. (2013) Study on isothermal kinetics of calcium barium sulphoaluminate mineral, *J. Inorg. Organomet. Polym. Mater.* 23, 1172-1176. http://dx.doi.org/10.1007/s10904-013-9883-0.
34. Rodrigues F.A. (2003) Synthesis of chemically and structurally modified dicalcium silicate, *Cem. Concr. Res.* 33 [6], 823-827. http://dx.doi.org/10.1016/S0008-8846(02)01065-7.
35. Wang S.D.; Huang Y.B.; Gong C.C.; Lu L.C.; Cheng X. (2014) Formation mechanism of barium calcium sulphoaluminate mineral, *Adv. Cem. Res.* 26 [3], 169-176. http://dx.doi.org/10.1680/adcr.13.00016.
36. Chang J.; Lu L.C.; Liu F.T.; Teng B.; Cheng X. (1999) Study on Ba-bearing calcium sulphoaluminate cement mineral, *J. Chin. Ceram. Soc.* 27, 644-650. http://dx.doi.org/10.14062/j.issn.0454-5648.1999.06.002.
37. Bhuiyan M.I.H.; Mavinic D.S.; Beckie R.D. (2008) Nucleation and growth kinetics of struvite in a fluidized bed reactor, *J. Cryst. Growth.* 310 [6], 1187-1194. http://dx.doi.org/10.1016/j.jcrysgro.2007.12.054.
38. Li X.R.; Zhang Y.; Shen X.D.; Wang Q.Q.; Pan Z.G. (2014) Kinetics of calcium sulphoaluminate formation from tricalcium aluminate, calcium sulfate and calcium oxide, *Cem. Concr. Res.* 55, 79-87. http://dx.doi.org/10.1016/j.cemconres.2013.10.006.